RESEARCH   **Open Access**

A joint DOA and polarization estimation method based on the conformal polarization sensitive array from the sparse reconstruction perspective

Xiaoyu Lan, Lai Jiang* and Peng Xu

*Correspondence:
jiang_lai0819@163.com

School of Electronic Information
Engineering, Shenyang
Aerospace University, Shenyang,
China

Abstract

The conformal polarization sensitive array (CPSA) is formed by placing some vector sensors on the conformal array and it has a wide range of practical application in direction of arrival (DOA) and polarization parameters estimation. However, due to the diversity of each sensor's direction, the performance of the conventional parameters estimation methods based on the CPSA would decrease greatly, especially under the low signal to noise ratio (SNR) and limited snapshots. In order to solve this problem, a unified framework and sparse reconstruction perspective for joint DOA and polarization estimation based on CPSA is proposed in this paper. Specifically, the array received signal model of the CPSA is formulated first and the two-dimensional spatial sparsity of the incident signals is then exploited. Subsequently, after employing the singular value decomposition method to reduce the dimension of array output matrix, the variational sparse Bayesian learning and orthogonal matching pursuit methods are utilized to solve the source DOA estimation, respectively. Finally, the polarization parameters are obtained by the minimum eigenvector method. Simulation results demonstrate that the novel approaches can provide improved estimation accuracy and resolution with low SNR and limited snapshots.

Keywords: Radar array signal processing, Conformal array, Polarizaiton sensitive array, Direction of arrival (DOA) and, Sparse reconstruction

1 Introduction

The joint direction-of-arrival (DOA) and polarization estimation of the polarization sensitive array (PSA) is one of the classical topics in array signal processing and has been widely used in radar, telecommunications, seismology [1]. In most scenarios, these estimation methods are proposed based on the linear array or planar array. Recently, the conformal array has aroused great concern. A conformal array [2, 3] is generally an array amounted with radiating sensors on the curvature surface. The conformal array has many benefits including reduction of aerodynamic drag, wide angle coverage, space saving, reduction of radar cross-section and so on. Complicated surface structure of CPSA

Lan *et al. EURASIP Journal on Advances in Signal Processing*   (2022) 2022:93

Page 2 of 18

will lead to the non-uniformity of element pattern and polarization characteristics, which brings lots of new challenges to parameters estimation. Therefore, the research on parameters estimation of CPSA is relatively significant.

At present, the DOA and polarization estimation methods based on the conformal array or the PSA are mainly according to their similar characteristics with the conventional array signal model and extended from the traditional parameter estimation techniques to conformal and PSA array. As a result, various approaches for cylindrical conformal arrays have been suggested to carry out two-dimensional (2D) DOA estimation, such as multiple signal classification (MUSIC) [4] and signal parameters via rotational invariance technique (ESPRIT) methods [5]. However, due to the direction diversity of the antenna, these conventional methods demand large signal to noise ratio (SNR) and snapshots. In practical electromagnetic environment, the increasingly dense signals and jamming signals, and more mobility targets will cause the received signal to face the problems of low SNR and small snapshots, which would cause the algorithm performance to deteriorate or even fail. In order to solve this problem, by considering the multidimensional structure of the array received data, the tensor technique is utilized to the MUSIC algorithm for cylindrical conformal array to improve the estimation performance [6, 7] proposed a 2D DOA estimation method by using the nested array on the cylindrical conformal arrays, which shows better performance. Nonetheless, the method in [6] is computationally much expensive as it requires spectrum peak searching, while the method in [7] needs to place the antenna in an elaborate design.

Recently, the emerging sparse reconstruction methods for DOA estimation, including ℓ_p-norm ($0 \leq p \leq 1$) methods [8–12], orthogonal matching pursuit (OMP) methods [13, 14] and the sparse Bayesian learning (SBL) methods [15–18], have aroused a lot of attention in DOA estimation. The essential idea of these algorithms is that the directions of incident source are substantially sparse in the spatial domain, which is intrinsically different from the subspace-based algorithms. Related methods have been shown to gain much enhanced performance over the subspace-based methods in the condition of low SNR and limited snapshots. In [19], a joint DOA, power and polarization estimation method using the cocentered orthogonal loop and dipole array is proposed by utilizing the signal reconstruction method. By exploiting the sparsity of the incident signals in the spatial domain, [20] proposed a novel method to estimated the DOA and polarization parameters by using SBL method. In [21], a novel off-grid hierarchical block-sparse Bayesian method for DOA and polarization parameters estimation was presented to improve the estimation accuracy [22]. Addressed a DOA and polarization estimation method based on the spatially separated polarization sensitive array under the SBL framework. However, these methods mentioned above focus on the estimation problem based on linear array or planar array, and do not consider the CPSA. As a result, the DOA and polarization estimation based on sparse reconstruction framework for CPSA needs further research.

This paper follows sparse reconstruction to address the joint DOA and polarization estimation based on the CPSA. By using the 2D joint sparsity signals of incident signals, a comprehensive array model is established first and a singular value decomposition (SVD) method is then used to reduce the dimension of array output matrix. And then, a variational sparse Bayesian learning (VSBL)-based method named

CPSA-VSBL and OMP-based method named CPSA-OMP are proposed to realize DOA estimation. Finally, the polarization parameters are obtained by the minimum eigenvector method. The scenario when cylinder CPSA is taken as example, so as to show how the CPSA-VSBL and CPSA-OMP realize DOA and polarization estimation jointly. Numerical examples also be provided to show how the performance of the proposed methods in DOA and polarization estimation and resolution under low SNR and limited snapshots.

Notations: Bold-italic letters are used to represent vectors and matrices. Lower case letters denotes scalars. $\mathcal{C}$ denotes complex numbers. $(\cdot)^{-1}$, $(\cdot)^{\mathrm{T}}$ and $(\cdot)^{\mathrm{H}}$ denote the inverse operation, transpose operation and conjugate transpose operation, respectively. $\langle \cdot \rangle$ denotes the statistical expectation. $\bullet$, $\otimes$ and $\odot$ denote Hadamard Product, Kronecker product and Khatri-Rao Product, respectively. For a vector $\boldsymbol{x}$, $\mathrm{diag}(\boldsymbol{x})$ is diagonal matrix with $\boldsymbol{x}$ being its diagonal. $\|\cdot\|_2$ represents 2-norm.

2 2D sparse signal model

As shown in Fig. 1, suppose that there are K narrowband far-field true sources $(\theta_k, \varphi_k, \gamma_k, \eta_k), k = 1, 2, \cdots, K$, impinging on an arbitrary CPSA with M electromagnetic vector sensor (EMVS), where θ_k is azimuth and φ_k is elevation, $\gamma_k \in [0, \pi/2)$ and $\eta_k \in [-\pi, \pi)$ are the polarization auxiliary angle and polarization phase difference angle of the k-th signal, respectively. $\boldsymbol{r}_i = [x_i, y_i, z_i]^{\mathrm{T}}, i = 1, 2, \cdots, M$ is position vector of i-th sensor. The propagation direction vector of the signal is $\boldsymbol{u} = [\sin\theta\cos\varphi, \sin\theta\sin\varphi, \cos\theta]^{\mathrm{T}}$. Each EMVS can output three electric-field vectors $\boldsymbol{E} = [\boldsymbol{e}_x, \boldsymbol{e}_y, \boldsymbol{e}_z]$ and three magnetic-field vectors $\boldsymbol{H} = [\boldsymbol{h}_x, \boldsymbol{h}_y, \boldsymbol{h}_z]$ [23]. For the k-th fully polarization wave, the polarization steering vector of each sensor can be written as
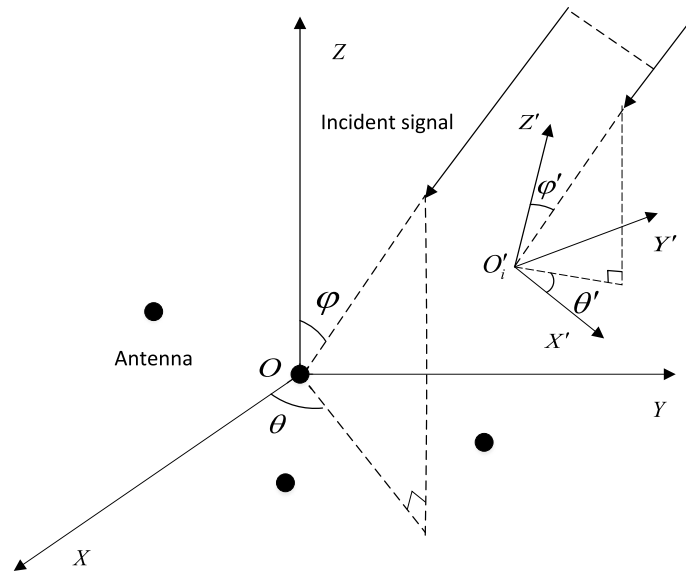
Fig. 1 Arbitrary conformal polarization sensitive array

$$
\begin{aligned}
\boldsymbol{b}(\theta_k, \varphi_k, \gamma_k, \eta_k) &= \begin{bmatrix} \boldsymbol{E}_k & \boldsymbol{H}_k \end{bmatrix}^{\mathrm{T}} \\
&= \begin{bmatrix} e_{xk} & e_{yk} & e_{zk} & h_{xk} & h_{yk} & h_{zk} \end{bmatrix}^{\mathrm{T}} \\
&= \begin{bmatrix}
\cos\varphi_k \cos\theta_k & -\sin\varphi_k \\
\sin\varphi_k \cos\theta_k & \cos\varphi_k \\
-\sin\theta_k & 0 \\
-\sin\varphi_k & -\cos\varphi_k \cos\theta_k \\
\cos\varphi_k & -\sin\varphi_k \cos\theta_k \\
0 & \sin\theta_k
\end{bmatrix}
\begin{bmatrix} \sin\gamma_k e^{j\eta_k} \\ \cos\gamma_k \end{bmatrix}, \\
&= \boldsymbol{v}(\theta_k, \varphi_k)\boldsymbol{\rho}(\gamma_k, \eta_k)
\end{aligned}
\tag{1}
$$

where $\boldsymbol{b}(\theta_k, \varphi_k, \gamma_k, \eta_k) \in \mathcal{C}^{6\times1}$, $\boldsymbol{v}(\theta_k, \varphi_k)$ and $\boldsymbol{\rho}(\gamma_k, \eta_k)$ represent the source's spatial information and polarization information, respectively.

$O(X, Y, Z)$ represents the global coordinate system in Fig. 1, and accordingly, $O'_i(X', Y', Z')$ represents the local coordinate system of i-th element [24]. Hence, θ is azimuth and φ is elevation in the global coordinate system, and accordingly, θ' and φ' are azimuth and elevation in the local coordinate system, respectively. Given the effect of the CPSA curvature, the element pattern and polarization characteristics of each sensor is not uniform any more. There exists a rotation matrix $\boldsymbol{R}$ in [25], so that the pattern of i-th sensor can be transformed from local coordinate system $g_i(\theta', \varphi')$ to global coordinate system $g_i(\theta, \varphi)$. Therefore, the array steering vector of the k-th signal can be written as

$$
\begin{aligned}
\bar{\boldsymbol{a}}(\theta_k, \varphi_k, \gamma_k, \eta_k) &= \boldsymbol{g}(\theta_k, \varphi_k) \bullet \boldsymbol{a}(\theta_k, \varphi_k) \odot \boldsymbol{b}(\theta_k, \varphi_k, \gamma_k, \eta_k) \\
&= \boldsymbol{d}(\theta_k, \varphi_k) \odot \boldsymbol{b}(\theta_k, \varphi_k, \gamma_k, \eta_k),
\end{aligned}
\tag{2}
$$

where $\boldsymbol{a}(\theta_k, \varphi_k) \in \mathcal{C}^{M\times1}$ denotes the spatial steering vector, $\boldsymbol{g}(\theta_k, \varphi_k) \in \mathcal{C}^{M\times1}$ denotes the element pattern in the global coordinate system. $\boldsymbol{d}(\theta_k, \varphi_k) = \boldsymbol{g}(\theta_k, \varphi_k) \bullet \boldsymbol{a}(\theta_k, \varphi_k)$ and its expression is formulated as follows

$$
\boldsymbol{d}(\theta_k, \varphi_k) = \left[g_1(\theta, \varphi)e^{-j\frac{2\pi}{\lambda}\boldsymbol{r}_1 \bullet \boldsymbol{u}_k}, \cdots, g_M(\theta, \varphi)e^{-j\frac{2\pi}{\lambda}\boldsymbol{r}_M \bullet \boldsymbol{u}_k} \right]^{\mathrm{T}},
\tag{3}
$$

$$
g_i(\theta, \varphi) = |f_i||e| \cos\left(\theta_{ife}\right) = \boldsymbol{f}_i \cdot \boldsymbol{e} = g_{i\theta}k_\theta + g_{i\varphi}k_\varphi, \quad i = 1, 2, ..., M,
\tag{4}
$$

$$
\boldsymbol{r}_i = [x_i, y_i, z_i]^{\mathrm{T}}, \quad i = 1, 2, \cdots, M,
\tag{5}
$$

$$
\boldsymbol{u}_k = [\sin\theta_k \cos\varphi_k, \sin\theta_k \sin\varphi_k, \cos\theta_k]^{\mathrm{T}},
\tag{6}
$$

where λ is the carrier wavelength. As shown in Fig. 2 [26], f_i is the direction diagram of the i-th sensor, u_θ and u_φ are unit vectors, k_θ and k_φ are the polarization parameters of the true sources. $g_{i\theta}$ and $g_{i\varphi}$ are the response of i-th sensor to the θ' and φ' in the local coordinate system [27]. Thus, the received data model is expressed as

$$
\bar{\boldsymbol{x}}(t) = \sum_{k=1}^{K} \bar{\boldsymbol{a}}(\theta_k, \varphi_k, \gamma_k, \eta_k)\bar{s}_k(t) + \bar{\boldsymbol{n}}(t),
\tag{7}
$$

where $\bar{\boldsymbol{x}}(t) = [\bar{x}_1(t), \cdots, \bar{x}_{6M}(t)]^{\mathrm{T}} \in \mathcal{C}^{6M\times1}$ and $\bar{\boldsymbol{n}}(t) = [\bar{n}_1(t), \cdots, \bar{n}_{6M}(t)]^{\mathrm{T}} \in \mathcal{C}^{6M\times1}$ are the received data vector and complex Gaussian noise vector, respectively. Consider
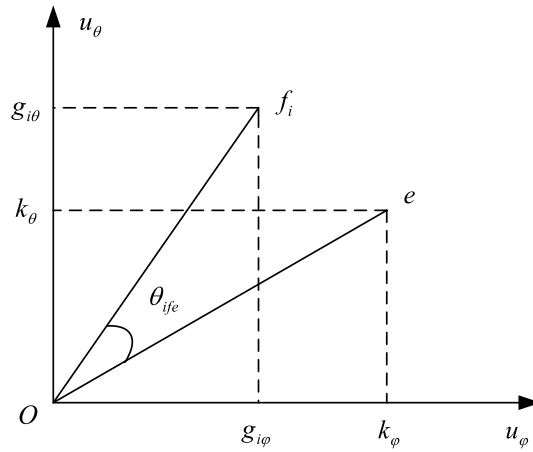
Fig. 2 Response of sensor

that all the K true sources are incident on the CPSA [28]. As a result, the array steering matrix is

$$
\begin{aligned}
\bar{A}(\theta,\varphi,\gamma,\eta) &= G(\theta,\varphi) \bullet A(\theta,\varphi) \odot B(\theta,\varphi,\gamma,\eta) \\
&= D(\theta,\varphi) \odot B(\theta,\varphi,\gamma,\eta) \\
&= D(\theta,\varphi)I \odot V(\theta,\varphi)Q(\gamma,\eta) \\
&= (D(\theta,\varphi) \otimes V(\theta,\varphi))(I \otimes Q(\gamma,\eta))
\end{aligned}
\tag{8}
$$

where $D(\theta,\varphi) = G(\theta,\varphi) \bullet A(\theta,\varphi)$ and $B(\theta,\varphi,\gamma,\eta) = V(\theta,\varphi)Q(\gamma,\eta)$. I is the $K \times K$ identity matrix. $\bar{A}$ is a $6M \times K$ matrix denoting the response of the array. It is seen that G denotes $M \times K$ element pattern matrix of K signals, A denotes the $M \times K$ full-rank steering matrix, B denotes the $6 \times K$ polarization steering matrix, $V(\theta,\varphi)$ denotes $6 \times 2K$ spatial information matrix of B, $Q(\gamma,\eta)$ denotes $2K \times K$ polarization information matrix of B.

$$
G(\theta,\varphi) = [g(\theta_1,\varphi_1), \cdots, g(\theta_K,\varphi_K)],
\tag{9}
$$

$$
A(\theta,\varphi) = [a(\theta_1,\varphi_1), \cdots, a(\theta_K,\varphi_K)],
\tag{10}
$$

$$
\begin{aligned}
B(\theta,\varphi,\gamma,\eta) &= [b(\theta_1,\varphi_1,\gamma_1,\eta_1), \cdots, b(\theta_K,\varphi_K,\gamma_K,\eta_K)] \\
&= [v(\theta_1,\varphi_1)\rho(\gamma_1,\eta_1), \cdots, v(\theta_K,\varphi_K)\rho(\gamma_K,\eta_K)]
\end{aligned}
\tag{11}
$$

$$
D(\theta,\varphi) = [d(\theta_1,\varphi_1), d(\theta_2,\varphi_2), \cdots, d(\theta_K,\varphi_K)]
\tag{12}
$$

$$
V(\theta,\varphi) = [v(\theta_1,\varphi_1), \cdots, v(\theta_K,\varphi_K)],
\tag{13}
$$

$$
Q(\gamma,\eta) = \mathrm{diag}(\rho(\gamma_1,\eta_1), \cdots, \rho(\gamma_K,\eta_K)).
\tag{14}
$$

Hence, the received array data model is given by

$$\bar{X}(t) = \bar{A}(\theta, \varphi, \gamma, \eta)\bar{S}(t) + \bar{N}(t), \tag{15}$$

For simplicity, (15) can be rewritten as

$$\bar{X} = \bar{A}\bar{S} + \bar{N}, \tag{16}$$

where $\bar{S} = [s_1, s_2, \cdots, s_K]^{\mathrm{T}}$, $\bar{N} = [n_1, n_2, \cdots, n_{6M}]^{\mathrm{T}}$. $\bar{S}$ and $\bar{N}$ denote $K \times T$ source and $6M \times T$ additive white Gaussian noise, respectively.

In order to use sparse reconstruction method to DOA estimation, generally [29], we can uniformly sample the range of azimuth and elevation to formulate a DOA set $\left\{ \left(\tilde{\theta}, \tilde{\varphi}\right)\right\} = \left\{ \left(\tilde{\theta}_1, \tilde{\varphi}_1\right), \cdots, \left\{ \left(\tilde{\theta}_{J_{\tilde{\theta}}}, \tilde{\varphi}_{J_{\tilde{\varphi}}}\right)\right\}\right\}$ with $J = J_{\tilde{\theta}}J_{\tilde{\varphi}} \gg K$. Assume that all the true sources lie on a fixed DOA set. For simplicity, the sparsity of the polarization information is not considered. The proposed methods are derived in the multiple measurement vectors. Therefore, the observation matrix X with the snapshots is T can be presented as

$$X = \tilde{A}S + N, \tag{17}$$

It is noted that $\tilde{A}$ is called the overcomplete dictionary and the number of $\tilde{A}$ columns is much larger than that of rows. Similar to (8), it can be found that $\tilde{A}$ not only depends spatial parameters but also depends polarization parameters. S is called sparse direction weights, each sparse weight has non-zero value only at the true source directions. Compared with nonsparse method, sparse reconstruction method can obtain the the source targets DOA with smaller reconstruction error. It expolits the observation matrix to reconstruct the signals and then the reconstructed signals are used to realize the DOA and polarization parameters estimation.

3 Methods

The sparse reconstruction methods [30, 31] make use of the sparsity of signal in the spatial domain to reconstruct true signals. In this section, we propose a sparsity-prompting CPSA-VSBL method to realize DOA estimation based on the MMV array output formulation given in (17). Meanwhile, the CPSA-OMP method is also proposed.

3.1 Dimensionality reduction of received data

From (17), it is easy to note that the large dimension of the received data will degrade the computational efficiency. So, SVD is conducted on X, we have

$$X = U\Sigma V^{\mathrm{H}}, \tag{18}$$

where U, Σ and V is denoted as the left singular matrix, eigenvalue matrix and right singular matrix, respectively. Let $V = [V_1, V_2]$, V is divided into V_1 and V_2 matrix according to the first K and the rest $T - K$ columns. In the presence of noise, we have $XV = [X_{\mathrm{sv}}, XV_2]$ by the SVD, where X_{sv} preserves most true sources information while the XV_2 is abandoned. Denote $Y = X_{\mathrm{sv}}$, $S_{\mathrm{sv}} = SV_1$ and $N_{\mathrm{sv}} = NV_1$, then we have

$$Y = \tilde{A}S_{\mathrm{sv}} + N_{\mathrm{sv}}, \tag{19}$$

where S_{sv} and N_{sv} are the new matrices of sparse direction weights and measurement noise, respectively. $Y \in \mathcal{C}^{6MK^2 \times K}$ represents the observation data matrix after reducing

the dimension of X, and $K \leq T$. Hence, by using Y in the following signal reconstruction process, the computational complexity of the algorithm is reduced greatly.

3.2 The proposed CPSA-VSBL method

The posterior distributions of all unknown parameters can be calculated by using the Bayesian criterion [32], we have

$$p(S_{\mathrm{sv}}, \alpha, \beta | Y) = \frac{p(Y, S_{\mathrm{sv}}, \alpha, \beta)}{p(Y)}. \tag{20}$$

Assume that all the variables are mutually independent, the joint probability density function (PDF) $p(Y, S_{\mathrm{sv}}, \alpha, \beta)$ is expressed as

$$p(Y, S_{\mathrm{sv}}, \alpha, \beta) = p\left(Y | S_{\mathrm{sv}}, \sigma^2\right) p(S_{\mathrm{sv}} | \alpha) p(\alpha | \tau, \beta) p(\beta | \nu), \tag{21}$$

where α and β are hyperparameters, $\tau \geq 0$ is shape parameter and $\nu \geq 0$ denotes rate parameter. The directed graphical model [33] of the factorization of the joint PDF is depicted in Fig. 3. N_{sv} obeys complex zero-mean stationary Gaussian noise with known variance σ^2. Thus, we have

$$p\left(N_{\mathrm{sv}} | \sigma^2\right) = \prod_{t=1}^{K} \mathcal{CN}\left(n_{\mathrm{sv}}(t) | 0, \sigma^2 I\right). \tag{22}$$

As a result, a Gaussian likelihood function model of Y can be obtained by

$$p\left(Y | S_{\mathrm{sv}}, \sigma^2\right) = \prod_{t=1}^{K} \mathcal{CN}\left(Y(t) | \tilde{A} S_{\mathrm{sv}}(t), \sigma^2 I\right). \tag{23}$$

The non-zero rows of S_{sv} contain all the angular information of the incident signals. The CPSA-VSBL method is employed to update the hidden variables and hyperparameters to approximate the posterior probability [34]. We apply a three-layer hierarchical prior [35] to S_{sv}. A zero-mean complex Gaussian (Gauss) distribution imposed on S_{sv} as the first layer of prior

$$p(S_{\mathrm{sv}} | \alpha) = \prod_{t=1}^{K} \mathcal{CN}\left(S_{\mathrm{sv}}(t) | 0, \Lambda^{-1}\right) = \prod_{t=1}^{K} \prod_{j=1}^{J} \mathcal{CN}\left(s_{\mathrm{sv}}(t)_j | 0, \alpha_j\right), \tag{24}$$

where $\Lambda^{-1} = \mathrm{diag}\left(1/\alpha_1, 1/\alpha_2, \cdots, 1/\alpha_j, \cdots, 1/\alpha_J\right)$, $\alpha_j = \sigma_j^{-2}$ and α_j is the j-th noise precision. The exponential (Exp) distribution is applied to the hyperparameter α as the second-layer prior
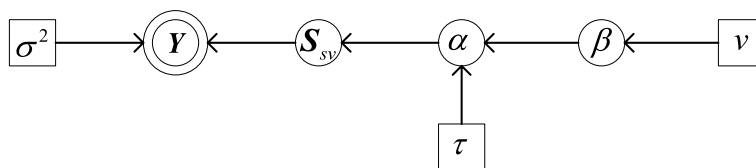
Fig. 3 Block diagram of variational Bayesian principle

$$p(\boldsymbol{\alpha}|\tau,\beta) = \prod_{j=1}^{J} Exp(\alpha_j|\tau,\beta). \tag{25}$$

The hyperparameter β obeys the chi-square (Chi2) distribution as the third-layer prior

$$p(\beta|\nu) = \chi^2(\beta|\nu). \tag{26}$$

However, $p(\boldsymbol{S}_{\mathrm{sv}},\boldsymbol{\alpha},\beta|\boldsymbol{Y})$ is not easy to solve. CPSA-VSBL minimizes Kullback-Leibler (KL) divergence [36] between approximate PDF $q(\Theta)$ and its posterior $p(\boldsymbol{S}_{\mathrm{sv}},\boldsymbol{\alpha},\beta|\boldsymbol{Y})$, where $\Theta = \{\boldsymbol{S}_{\mathrm{sv}},\boldsymbol{\alpha},\beta\}$. The independent variables in $q(\Theta)$ can be rewritten into the product form of the distribution function which is described as $q(\Theta) = q(\boldsymbol{S}_{\mathrm{sv}},\boldsymbol{\alpha},\beta) = q(\boldsymbol{S}_{\mathrm{sv}})q(\boldsymbol{\alpha})q(\beta)$. We can get the mean, variance of $\boldsymbol{S}_{\mathrm{sv}}$, and hyperparameters through the following steps.

The posterior distribution $q(\boldsymbol{S}_{\mathrm{sv}})$ is updated by $q(\boldsymbol{S}_{\mathrm{sv}}) \propto (p(\boldsymbol{Y},\boldsymbol{S}_{\mathrm{sv}},\boldsymbol{\alpha},\beta))_{q(\boldsymbol{\alpha})}$, where $(\cdot)_{q(\boldsymbol{\alpha})}$ denotes the subset of Θ that removes $\boldsymbol{\alpha}$. $p(\boldsymbol{Y},\boldsymbol{S}_{\mathrm{sv}},\boldsymbol{\alpha},\beta)$ can be obtained by the joint distribution of $p(\boldsymbol{Y}|\boldsymbol{S}_{\mathrm{sv}})$ and $p(\boldsymbol{S}_{\mathrm{sv}}|\boldsymbol{\alpha})$. We can acquire the approximate posterior for $q(\boldsymbol{S}_{\mathrm{sv}})$ as

$$q(\boldsymbol{S}_{\mathrm{sv}}) = \prod_{t=1}^{K} \mathcal{CN}(\boldsymbol{S}_{\mathrm{sv}}(t)|\mu(t),\Gamma). \tag{27}$$

The parameters of the approximate posterior in (27) can be renewed according to

$$\mu(t) = \sigma^{-2}\Gamma^{-1}\tilde{\boldsymbol{A}}^{\mathrm{H}}\boldsymbol{Y}(t), \tag{28}$$

$$\Gamma = \left(\sigma^{-2}\tilde{\boldsymbol{A}}^{\mathrm{H}}\tilde{\boldsymbol{A}} + \langle \Lambda \rangle\right)^{-1}, \tag{29}$$

The $q(\boldsymbol{\alpha})$ is updated according to $q(\boldsymbol{\alpha}) \propto (p(\boldsymbol{S}_{\mathrm{sv}}|\boldsymbol{\alpha})p(\boldsymbol{\alpha}|\tau,\beta))_{q(\boldsymbol{S}_{\mathrm{sv}})q(\beta)}$ and can be approximated as the product of the PDF of the generalized inverse Gaussian distribution, and thus, we have

$$\left\langle \alpha_j^n \right\rangle = \left(\frac{\left\langle h_j^2 \right\rangle}{2\tau\langle\beta\rangle} \right)^{\frac{n}{2}} \frac{\kappa_{\frac{n-1}{2}}\left(\sqrt{2\tau\langle\beta\rangle\left\langle h_j^2\right\rangle}\right)}{\kappa_{-\frac{1}{2}}\left(\sqrt{2\tau\langle\beta\rangle\left\langle h_j^2\right\rangle}\right)}, \tag{30}$$

where $\left\langle h_j^2 \right\rangle = \mu_j^2 + \Gamma_j$, $\kappa_p(\cdot)$ is referred to the third kind Bessel function with order p. When $n = -1$, the estimated Γ and $\langle\Lambda\rangle$ in (29) are obtained.

The posterior distribution $q(\beta)$ is updated by $q(\beta) \propto (p(\alpha|\tau,\beta)p(\beta|\nu))_{q(\alpha)}$ and complies with Gamma distribution as

$$\beta \sim \mathrm{Gamma}\left(J + \frac{\nu}{2}, \tau\sum_{j=1}^{J}\langle\alpha_j\rangle + \frac{1}{2}\right). \tag{31}$$

Thus, the mean value of β can be expressed as

Table 1 The execution steps of CPSA-VSBL algorithm

Algorithm:CPSA-VSBL
Input:the steering matrix $\tilde{A}$,observation data matrix Y
1.**Initialization**:$\langle \alpha_j \rangle$, $\langle \alpha_j^{-1} \rangle$, $\langle \beta \rangle$, τ, ν, σ^2, ε, $i_{\max}$
2.while not converged do
3.   Update $\Gamma^{(i)}$ by (29)
4.   Update $\mu^{(i)}$ by (28)
5.   Update $\langle \alpha_j \rangle^{(i)}$ by (30)
6.   Update $\langle \beta \rangle^{(i)}$ by (32)
7.end while
Output:The mean μ and variance Γ of the recovery signal

Table 2 The execution steps of CPSA-OMP algorithm

Algorithm:CPSA-OMP
Input:Y, $\tilde{A}$, K
1. **Initialization**: residual $w^0 = Y$, $res^0 = \phi$, where ϕ denotes null index set.
2. for $i=1$ to K
3.   Find the index corresponding to the maximization inner product: $res^i = \arg\max_i \left\| \tilde{A} w^{i-1} \right\|$
4.   Update the index set: $res^i = res^{i-1} \cup res^i$
5.   Calculate the least square solution of (33):$Y_{res^i} = \left(\tilde{A}_{res^i}^H \tilde{A}_{res^i} \right)^{-1} \tilde{A}_{res^i}^H Y$
6.   Update the residual: $w^i = Y - \tilde{A}_{res^i}^i Y_{res^i}$
7.end for
Output: w^i, Y_{res^i}

$$\langle \beta \rangle = \frac{J + \frac{\nu}{2}}{\tau \sum_{j=1}^{J} \langle \alpha_j \rangle + \frac{1}{2}}. \tag{32}$$

CPSA-VSBL firstly carries out the initialization of constant variables in the selected distribution function, and then iteratively update the hidden variables and hyperparameters in turn until the set convergence conditions are satisfied [37]. The CPSA-VSBL algorithm in this paper is summarized in Table 1.

3.3 The proposed CPSA-OMP method

In the CPSA-OMP method, S can be reconstructed from the known matrix Y and $\tilde{A}$ based on the idea of dictionary atomic matching. In each iteration of CPSA-OMP, a column of $\tilde{A}$ is selected by orthogonal projection method, which is most relevant to the Y. Then we subtract off its contribution to Y and iterate over the remaining residual $w_{res^i}^i$. The algorithm will identify the index set of the correct column when the residual is zero. The minimization of $w_{res^i}^i$ is selected by as follows

$$w_{res^i}^i = \arg\min_{Y_{res^i}} \left\| Y - \tilde{A}_{res^i}^i Y_{res^i} \right\|_2^2, \tag{33}$$

where $w_{res^i}^i$ is the residual matrix in the i-th iteration, $\tilde{A}_{res^i}^i$ denotes the remaining part of $\tilde{A}$ after the i-th iteration. The execution steps of CPSA-OMP algorithm are shown in Table 2.

Some remarks of specific implementation of CPSA-VSBL and CPSA-OMP are shown as follows.

Remark 1

The number of target sources K is used as known condition. Estimation K as a significant study topic is outside the scope of this paper. Furthermore, the scenarios of coherent sources and colored noise are not considered.

Remark 2

Compared with the conventional two-layer prior, the CPSA-VSBL method benefits from the selected three-layer prior (Gauss-Exp-Chi2) with the property of a sharp peak at the origin and heavy tails. It has the effect of prompting the sparsity of its solutions.

Remark 3

In this paper, CPSA-VSBL and CPSA-OMP methods only discussed the CPSA-based structure. It is noted that the proposed methods can be generalized to arbitrary array geometries.

Remark 4

According to empirical, the hyperparameters α and β are initialized to the $\frac{1}{T}\sum_{t=1}^{K}\tilde{A}Y(t)$ and 0.1, respectively. $\tau = 1.5$ and $\nu = 1$ are set in the third level prior distribution. $\varepsilon = 10^{-3}$ and $i_{\max} = 2000$ represent the termination threshold and maximum iterative number, respectively.

3.4 Refined DOA estimation

The mean and variance of $\bar{S}$ can be output in $\{[\mu_1, \Gamma_1], [\mu_2, \Gamma_2], \cdots, [\mu_J, \Gamma_J]\}$ after the iteratively update termination criterion $\left\| \langle \alpha_j \rangle^{(i)} - \langle \alpha_j \rangle^{(i-1)} \right\| / \left\| \langle \alpha_j \rangle^{(i-1)} \right\| < \varepsilon$ or $i > i_{\max}$ is reached. The powers from different directions are obtained by substituting the estimated $[\mu, \Gamma]$ into the power function, where the power of the j-th impinging signal in the Ω is expressed as $\hat{P}_j$

$$\hat{P}_j = \frac{1}{L}\left\langle \left\| S_{sv_j} \right\|_2^2 \right\rangle = \frac{1}{L}\left(\left\| \langle S_{sv_j} \rangle \right\|_2^2 + \left\langle \left\| S_{sv_j} - \langle S_{sv_j} \rangle \right\|_2^2 \right\rangle \right) = \frac{\left\| \mu_j \right\|_2^2}{L} + \Gamma_j. \tag{34}$$

We use all the estimated signal powers to form a power spectrum. Similar to other spectral-searching-based methods, the DOA is estimated by finding the positions of the highest peaks of the spectrum. Suppose that the grid indices of the highest K power values are the position of the true sources. The estimated K DOA will be $\left\{ \left[\hat{\theta}_1, \hat{\varphi}_1 \right], \left[\hat{\theta}_2, \hat{\varphi}_2 \right], \cdots, \left[\hat{\theta}_K, \hat{\varphi}_K \right] \right\}$

3.5 The polarization parameters estimation

Consider that the true sources $\bar{S} = [s_1, s_2, \cdots, s_K]^{\mathrm{T}}$ impinge on the surface of the CPSA as shown in Fig. 1. Then the steering vector of the k-th source is

$$\hat{a}(\theta_k, \varphi_k, \gamma_k, \eta_k) = g(\theta_k, \varphi_k) \bullet \widehat{a}(\theta_k, \varphi_k) \odot b(\theta_k, \varphi_k, \gamma_k, \eta_k), \tag{35}$$

where $g(\theta_k, \varphi_k) = [g_1(\theta_k, \varphi_k), g_2(\theta_k, \varphi_k), \cdots, g_M(\theta_k, \varphi_k)]$, $g_i(\theta_k, \varphi_k)$ is the response of unit signal by the i-th array element to the k-th signal, and $\widehat{a}(\theta_k, \varphi_k) = \left[\mathrm{e}^{-j\frac{2\pi}{\lambda}u_k \bullet r_1}, \mathrm{e}^{-j\frac{2\pi}{\lambda}u_k \bullet r_2}, \ldots, \mathrm{e}^{-j\frac{2\pi}{\lambda}u_k \bullet r_M} \right]^{\mathrm{T}}$ is phase delay vector.

The array manifold matrix of the CPSA is shown as

$$\hat{A}(\theta, \varphi, \gamma, \eta) = \left[\hat{a}(\theta_1, \varphi_1, \gamma_1, \eta_1), \hat{a}(\theta_2, \varphi_2, \gamma_2, \eta_2), \cdots, \hat{a}(\theta_K, \varphi_K, \gamma_K, \eta_K) \right]. \tag{36}$$

The received data model of polarization parameters estimation could be written as

$$\hat{X} = \hat{A}\bar{S}. \tag{37}$$

In order to catch the noise subspace U_{N} of $\hat{X}$, by taking the eigenvalue decomposition of the covariance matrix $R = \frac{1}{L}\hat{X}\hat{X}^{\mathrm{H}}$ and let the K eigenvectors corresponding to the K significant eigenvalues to form the signal subspace U_{S}. Hence, U_{N} can be expressed as

$$U_{\mathrm{N}} = I_{\mathrm{MT}} - U_{\mathrm{S}}U_{\mathrm{S}}^{\mathrm{H}}, \tag{38}$$

where I_{MT} symbolizes $MT \times MT$ identity matrix. The K estimated DOA in section 3.4 are substituted into the constructed conventional spatial spectrum function to obtain the K functions as follows

$$W = \frac{1}{\hat{A}^{\mathrm{H}}(\theta, \varphi, \gamma, \eta)U_N\hat{A}(\theta, \varphi, \gamma, \eta)}. \tag{39}$$

The polarization parameters can be calculated by the eigenvector corresponding to the minimum eigenvalue of W [38].

$$\gamma_k = \arctan\left(\mathrm{abs}\left(\rho_k(2)/\rho_k(1)\right)\right), \tag{40}$$

$$\eta_k = \mathrm{angle}\left(\rho_k(2)/\rho_k(1)\right), \tag{41}$$

where $\rho_k(i)$ denotes the i-th element in the eigenvector.

4 The computational cost analysis

It is obviously that the proposed methods based on the sparse model will be more time consuming than the subspace-type methods. The reason is the dimension of the output matrix X in sparse signal model is too large to iteratively update the mean, variance and hyperparameters in (28), (29), (30) and (32) quickly. As a result, SVD is utilized to reduce the dimension of X to improve computational efficiency before the sparse component learning and inner product.

As far as the computational complexity, CPSA-VSBL in this paper mainly derives from solving for the hidden variables and hyperparameters. Among the mean and variance of S_{sv}

**Table 3** Comparison of computational load

Algorithms	Computation cost	O_t
MUSIC	$O_t\left(36M^2T + 216M^3 + n^2[6M(6M - K)]\right)$	$O_t\left(5.55 \times 10^{11}\right)$
Tensor-MUSIC	$O_t\left(36M^2T + 216M^3 + n^2[6M(6M - K)] + 10.67TMK\right)$	$O_t\left(5.55 \times 10^{11}\right)$
CPSA-OMP	$O_t(KMJ) + O\left(6MKT^2\right)$	$O_t\left(1.57 \times 10^6\right)$
CPSA-VSBL	$O_t\left(3J^3 - 2J^2 + 8J^2M + 4JM^2 + 2JMT + 6MKT^2\right)$	$O_t\left(1.35 \times 10^{13}\right)$
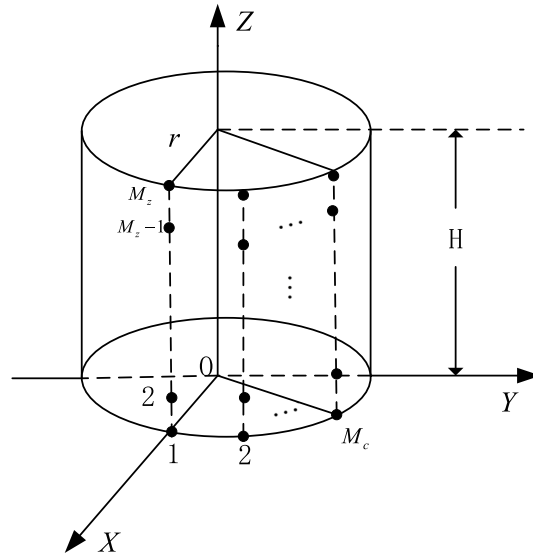
Fig. 4 Uniform cylinder CPSA

is approximately $2J^3 - 2J^2 + 6J^2M + 4JM^2 + M^3 - 3JM$ and $J^3 + 2J^2M + 2JMK - JM$, respectively. Then the hyperparameters $\langle\alpha_j\rangle$ and $\langle\alpha_j^{-1}\rangle (j = 1, 2, \cdots, J)$ are about $4J$ and $10J$. The most time consuming of the CPSA-OMP is the selection of atoms in the dictionary $\tilde{A}$, and the computational complexity of each inner product is MJ. An appended computational load for the SVD of X is $6MKT^2$. The computational complexity of covariance matrix and eigenvalue decomposition in Tensor-MUSIC and MUSIC is $36M^2T$ and $216M^3$, and the spectral searching of subspace methods is $n^2[6M(6M - K)]$. In addition to, Tensor-MUSIC also needs higher order singular value decomposition. The computational complexity of the above methods is given in Table 3 when an arbitrary conformal array with M=25, K=2, J=16471, T=50 and n=5000, where n is the number of angle searches. The computational complexity is represented as O_t.

5 Results and discussion

In this section, the simulation results of CPSA-VSBL and CPSA-OMP based on CPSA are analyzed, and compared with MUSIC and Tensor-MUSIC. As shown in Fig. 4, the array structure in the simulation is a cylindrical carrier and there are $M_c \times M_z$ sensors are uniformly distributed over the surface of the cylinder. The distance between the
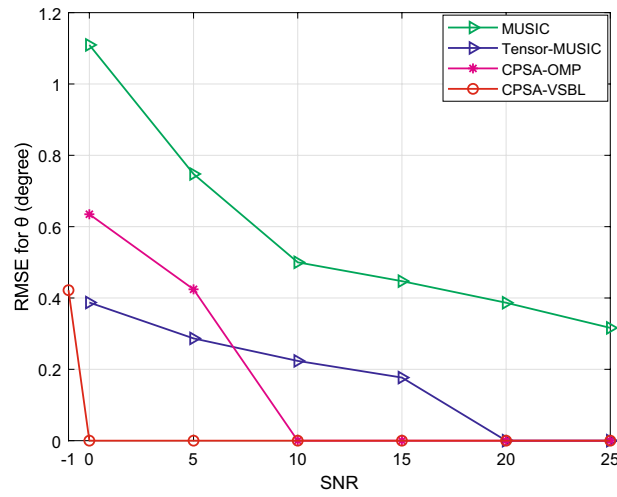
Fig. 5 The azimuth RMSE versus SNR
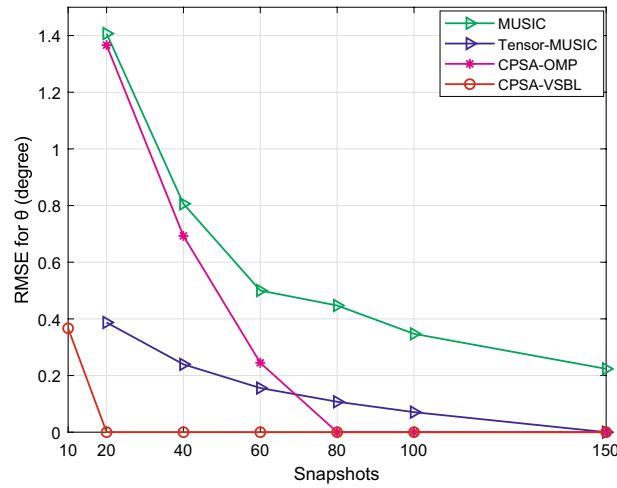
Fig. 6 The azimuth RMSE versus number of snapshots

adjacent sensors along the Z-axis is $\frac{\lambda}{2}$. For simplicity, we assume $M_z = 5$ and $M_c = 5$. The range of azimuth and elevation is sampled with $1°$ interval to form the direction set $\left\{ \left(\tilde{\boldsymbol{\theta}}, \tilde{\boldsymbol{\varphi}} \right) \right\}$. The RMSE of DOA estimation by independent Monte Carlo simulations is defined as

$$RMSE = \sqrt{\frac{1}{QK} \sum_{q=1}^{Q} \sum_{k=1}^{K} \left(\hat{u}_{kq} - u_k \right)^2}, \tag{42}$$

where Q denotes the number of Monte Carlo simulations, u_k is one of the parameters $(\theta_k, \varphi_k, \gamma_k, \eta_k)$, and $\hat{u}_{kq}$ is the estimation of u_k in the q-th simulation.

5.1 The estimation accuracy versus SNR and the number of snapshots

In this simulations, the DOA estimation accuracy is evaluated by RMSE. The RMSE of the DOA estimation methods versus the SNR and number of snapshots are shown in Figs. 5 and 6, respectively. Consider two uncorrelated incident signals with DOA and polarization parameters $(\theta, \varphi, \gamma, \eta)$ are $(-14°, 35°, 25°, 10°)$ and $(10°, 50°, 50°, 45°)$, respectively. The number of snapshots is fixed at 50. The RMSE versus SNR from -1 to 25 dB for the four methods is presented in Fig. 5, and the RMSE versus snapshots number from to 10 to 150 while SNR=5 dB is presented in Fig. 6. In each experiment, we run 300 Monte Carlo simulations. From Figs. 5 and 6, it can be seen that, the RMSE performance of four methods are improved with the SNR and snapshots increasing. In Fig. 5, the proposed CPSA-VSBL has a more accurate DOA estimation than other methods at every SNR. The performance of the proposed CPSA-OMP is apparently superior to MUSIC and Tensor-MUSIC while the SNR is relatively high. In Fig. 6, the proposed CPSA-VSBL offers the best performance than that of CPSA-OMP, MUSIC and Tensor-MUSIC. CPSA-OMP provides an estimation with zero error when the number of snapshots is relatively large. We further examine the RMSE of polarization parameters estimation. For all the methods, it can be seen that the RMSE continuously decrease when SNR and the number of snapshots increase. It is observed that the RMSE γ and η of the proposed methods consistently outperform the Tensor-MUSIC and MUSIC methods in Fig. 7. From Fig. 8, the estimation performance of the proposed CPSA-VSBL is better than subspace methods at arbitrary number of snapshots. The CPSA-OMP performs better than the MUSIC and Tensor-MUSIC methods in the large number of snapshots.

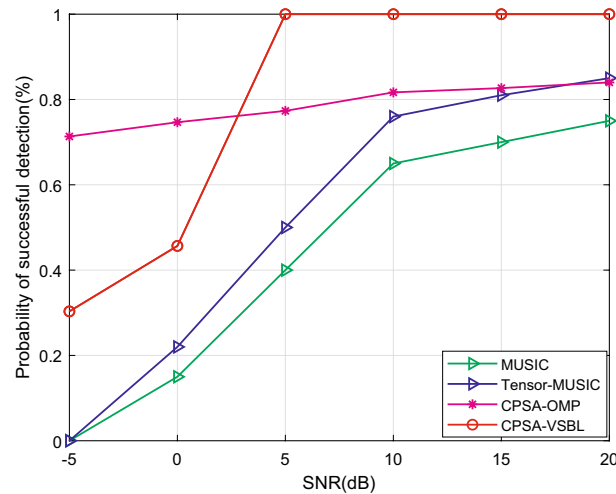### 5.2 The resolution performance versus SNR and number of snapshots

In this subsection, the resolution performance is evaluated by the probability of successful detection. For the MUSIC and Tensor-MUSIC methods, the "successful trial" is defined in this simulation as when both the $\left|\hat{\theta} - \theta\right| < 2°$ and $\left|\hat{\varphi} - \varphi\right| < 2°$. Set the two uncorrelated incident signals with DOA and polarization parameters $(\theta, \varphi, \gamma, \eta)$ are

**Fig. 7** The RMSE of γ and η versus SNR

Lan *et al. EURASIP Journal on Advances in Signal Processing* (2022) 2022:93

Page 15 of 18
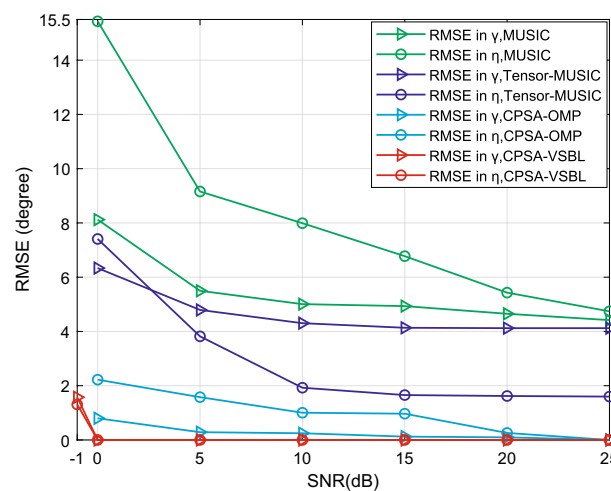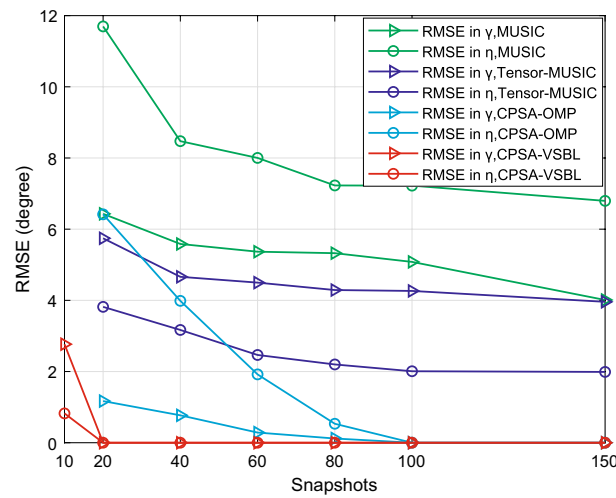
Fig. 8 The RMSE of γ and η versus number of snapshots

Fig. 9 The probability of successful detection versus SNR

$(-8°, 45°, 10°, 30°)$ and $(2°, 45°, 30°, 20°)$, respectively. Set the number of snapshots is 50, the probability of successful detection of four methods varying SNR from -5 to 20 dB in Fig. 9. Figure 10 shows the probability of successful detection for SNR=5 dB by varying the snapshots from 20 to 200 under the two uncorrelated incident signals with DOA and polarization parameters $(\theta, \varphi, \gamma, \eta)$ are $(-4°, 45°, 10°, 30°)$ and $(6°, 45°, 30°, 20°)$. It is seen from Figs. 9 and 10, both the probability of successful detection improve with the increasing of the SNR and the number of snapshots, whereas the proposed methods have higher resolution performance than the conventional MUSIC and Tensor-MUSIC methods, which gives us a strong evidence of the effectiveness of the proposed methods.
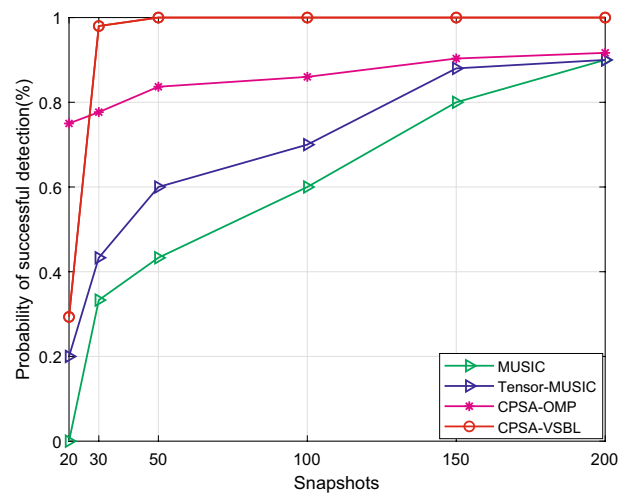
Fig. 10 The probability of successful detection versus number of snapshots

6 Conclusions

In this paper, we have illustrated sparse reconstruction method-based DOA and polarization joint estimation for CPSA. By exploiting 2D spatial sparsity of incident signals, an array output model that is applicable to arbitrary CPSA is obtained. In order to improve the computational efficiency of the proposed methods, SVD is used to reduce the dimension of the array output matrix. The CPSA-VSBL and CPSA-OMP methods are proposed for DOA estimation. The minimum eigenvector method is used to obtain the polarization information of signals. As a result, both the estimation accuracy and the resolution of the proposed methods have been validated by a lot of simulations. The simulation results show that the proposed methods have low RMSE and optimal resolution than the state-of-the-art methods especially with low SNR and limited snapshots. In future work, we will focus on the multidimensional structural information in the array received data.

Abbreviations

CPSA   Conformal polarization sensitive array
DOA   Direction of arrival
2D   Two-dimensional
SNR   Signal to noise ratio
VSBL   Variarional sparse Bayesian learning
OMP   Orthogonal matching pursuit
PSA   Polarization sensitive array
SBL   Sparse Bayesian learning
EMVS   Electromagnetic vector sensor
CPSA-VSBL   CPSA variational sparse Bayesian learning
CPSA-OMP   CPSA orthogonal matching pursuit
MUSIC   Multiple signal classification
ESPRIT   Estimation of signal parameters via rotational invariance techniques
RMSE   Root meansquare error
PDF   Probability density function
KL   Kullback-Leibler
SVD   Singular value decomposition

Declarations

Ethics approval and consent to participate
Not applicable.

Consent for publication
Not applicable.

Competing interests
The authors declare that they have no competing interests.

References
1. H. Krim, M. Viberg, Two decades of array signal processing research: the parametric approach. IEEE Signal Process. Mag. **13**(4), 67–94 (1996)
2. L. Josefesson, P. Persson, Conformal array antenna theory and design (josefsson/conformal array antenna theory and design) ‖ antennas on doubly curved surfaces. 10.1002/047178012X , 463-470 (2006)
3. Y. Gao, W. Jiang, W. Hu, Q. Wang, W. Zhang, A dual-polarized 2-D monopulse antenna array for conical conformal applications. IEEE Trans. Antennas Propag. **69**(9), 5479–5488 (2021)
4. P. Yang, F. Yang, Z. Nie, DOA estimation of cylindrical conformal array by MUSIC algorithm. Chin. J. Radio Sci. **23**(2), 288–291 (2008)
5. Z. Qi, Y. Gou, B. Wang, C. Gong, DOA estimation algorithm for conical conformal array antenna. 2009. in *IET international radar conference*, pp. 1-4 (2009)
6. X. Lan, L. Wang, Y. Wang, C. Choi, D. Choi, Tensor 2-D DOA estimation for a cylindrical conformal antenna array in a massive MIMO system under unknown mutual coupling. IEEE Access. **6**, 7864–7871 (2018)
7. M. Fu, Z. Zheng, W. Wang, Y. Liao, Two-dimensional direction-of-arrival estimation for cylindrical nested conformal arrays. Signal Process. **179**, 107838 (2021)
8. P. Bohra, M. Unser, Continuous-domain signal reconstruction using l_p-norm regularization. IEEE Trans. Signal Process. **68**, 4543–4554 (2020)
9. M. Zuo, S. Xie, X. Zhang, M. Yang, DOA estimation based on weighted l_1-norm sparse representation for low SNR scenarios. Sensors **21**(13), 4614 (2021)
10. X. Wu, W. Zhu, J. Yan, A high-resolution DOA estimation method with a family of nonconvex penalties. IEEE Trans. Veh Technol. **67**(6), 4925–4938 (2018)
11. J. Yin, T. Chen, Direction-of-arrival estimation using a sparse representation of array covariance vectors. IEEE Trans. Signal Process. **59**(9), 4489–4493 (2011)
12. H. Bai, M.F. Darte, R. Janaswamy, Direction of arrival estimation for complex sources through l_1-norm sparse Bayesian learning. IEEE Signal Process. Lett. **26**(5), 765–769 (2019)
13. W.S. Leite, R.C. de Lamare, List-based OMP and an enhanced model for DOA estimation with nonuniform arrays. IEEE Trans. Aerosp Electron Syst. **57**(6), 4457–4464 (2021)
14. X. Zhang, Y. Li, Y. Yuan, T. Jiang, in *2018 IEEE Asia-Pacific Conference on Antennas and Propagation (APCAP), Low-complexity DOA estimation via OMP and majorization-minimization*. (IEEE, Auckland, 2018), pp. 18-19
15. M. Fu, Z. Zheng, W. Wang, 2-D DOA estimation for nested conformal arrays via sparse reconstruction. IEEE Commun. Lett. **25**(3), 980–984 (2020)
16. S. Uemura, K. Nishimori, R. Taniguchi, M. Inomata, K. Kitao, T. Imai, S. Suyama, H. Ishikawa, Y. Oda, Direction-of-arrival estimation with circular array using compressed sensing in 20 GHz band. IEEE Antennas Wirel. Propag. Lett. **20**(5), 703–707 (2021)
17. P. Chen, Z. Cao, Z. Chen, X. Wang, Off-grid DOA estimation using sparse Bayesian learning in MIMO radar with unknown mutual coupling. IEEE Trans. Signal Process. **67**(1), 208–220 (2018)
18. Z. Yang, L. Xie, C. Zhang, Off-grid direction of arrival estimation using sparse Bayesian inference. IEEE Trans. Signal Process. **61**(1), 38–43 (2012)
19. Y. Tian, H. Xu, DOA, power and polarization angle estimation using sparse signal reconstruction with a COLD array. AEU-Int. J. Electron. Commun. **69**(11), 1606–1612 (2015)
20. Z. Liu, DOA and polarization estimation via signal reconstruction with linear polarization-sensitive arrays. Chin. J. Aeronaut. **28**(6), 1718–1724 (2015)

21. P. Zhao, G. Hu, H. Zhou, An Off-grid block-sparse Bayesian method for direction of arrival and polarization estimation. Circ. Syst. Signal Process. **39**(9), 4378–4398 (2020)
22. B. Li, W. Bai, G. Zheng, X. He, B. Xue, M. Zhang, BSBL-based DOA and polarization estimation with linear spatially separated polarization sensitive array. Wirel. Pers. Commun. **109**(3), 2051–2065 (2019)
23. Y. Hu, Y. Zhao, S. Chen, X. Pang, Two-dimensional DOA estimation of the conformal array composed of the single electric dipole under blind polarization. Digit. Signal Process. **122**, 103353 (2022)
24. C. Liu, F. Zhou, A mutiparameter joint estimation algorithm for dual-polarized cylindrical conformal array in the presence of mutual coupling. Int. J. Antennas Propag. 2022, (2022)
25. B. Wang, Y. Guo, *2008 international workshop on antenna technology: small antennas and novel metamaterials, array manifold modeling for arbitrary 3D conformal array antenna* (Japan, IEEE, 2008), pp.562–565
26. L. Wan, W. Si, L. Liu, Z. Tian, N. Feng, High accuracy 2D-DOA estimation for conformal array using PARAFAC. Int. J. Antennas Propag. 2014, (2014)
27. M. Gao, S. Zhang, M. Cao, Z. Liu, M. Li, in *2020 international conference on virtual reality and intelligent systems (ICVRIS), Joint estimation of DOA and polarization based on cylindrical conformal array Antenna*. (IEEE, Hunan, 2000), pp. 1052–1056
28. X. Lan, J. Wang, L. Jiang, in *2022 IEEE 5th international conference on electronics technology (ICET), joint DOA and polarization estimation of conformal electromagnetic vector array*. (IEEE, online, 2022), pp. 691–696
29. L. Liang, Y. Shi, Y. Shi, Z. Bai, W. He, Two-dimensional DOA estimation method of acoustic vector sensor array based on sparse recovery. Digit. Signal Process **120**, 103294 (2022)
30. J. Dai, H.C. So, Real-valued sparse Bayesian learning for DOA estimation with arbitrary linear arrays. IEEE Trans. Signal Process. **69**, 4977–4990 (2021)
31. S.D. Babacan, S. Nakajima, M.N. Do, Bayesian group-sparse modeling and variational inference. IEEE Trans. Signal Process. **62**(11), 2906–2921 (2014)
32. D.G. Tzikas, A.C. Likas, N.P. Galatsanos, The variational approximation for Bayesian inference. IEEE Signal Process. Mag. **25**(6), 131–146 (2008)
33. M.I. Jordan, Z. Ghahramani, T.S. Jaakkola, L.K. Saul, An introduction to variational methods for graphical models. Mach. learn. **37**(2), 183–233 (1999)
34. M.E. Tipping, Sparse Bayesian learning and the relevance vector machine. J. Mach. Learn. Res. **1**, 211–244 (2001)
35. P. Zhao, W. Si, G. Hu, L. Wang, DOA estimation for a mixture of uncorrelated and coherent sources based on hierarchical sparse Bayesian inference with a Gauss-Exp-Chi 2 prior. Int. J. Antennas Propag. **2018**, 1–12 (2018)
36. C.W. Fox, S.J. Roberts, A tutorial on variational Bayesian inference. Artif. Intell. Rev. **38**(2), 85–95 (2012)
37. B. Wang, D.M. Titterington, Convergence properties of a general algorithm for calculating variational Bayesian estimates for a normal mixture model. Bayesian Anal. **1**(1), 625–649 (2006)
38. C. Liu, Z. Fang, S. Xiang, in *2019 6th international conference on systems and informatics (ICSAI), joint polarization and space domain adaptive beamforming for dual polarized conformal array*. (IEEE, Shanghai, 2019), pp. 1126–1130

Publisher's Note

Springer Nature remains neutral with regard to jurisdictional claims in published maps and institutional affiliations.